BJP British Journal of Pharmacology

DOI:10.1111/bph.12807
www.brjpharmacol.org

Themed Section: Opioids: New Pathways to Functional Selectivity

RESEARCH PAPER

Specific regions display altered grey matter volume in μ-opioid receptor knockout mice: MRI voxel-based morphometry

Kazumasu Sasaki[1,2], Akira Sumiyoshi[2], Hiroi Nonaka[2], Yoshiyuki Kasahara[1], Kazutaka Ikeda[3], F Scott Hall[4], George R Uhl[4], Masahiko Watanabe[5], Ryuta Kawashima[2,6,7] and Ichiro Sora[1,8]

[1]*Department of Biological Psychiatry, Tohoku University Graduate School of Medicine, Sendai, Japan,* [2]*Department of Functional Brain Imaging,* [6]*Division of Developmental Cognitive Neuroscience,* [7]*Smart Ageing International Research Center, Institute of Development, Aging and Cancer, Tohoku University, Sendai, Japan,* [3]*Addictive Substance Project, Tokyo Metropolitan Institute of Medical Science, Tokyo, Japan,* [4]*Molecular Neurobiology Branch, National Institute on Drug Abuse-Intramural Research Program, National Institutes of Health, DHHS, Baltimore, MD, USA,* [5]*Department of Anatomy, Hokkaido University Graduate School of Medicine, Sapporo, Japan, and* [8]*Department of Psychiatry, Kobe University Graduate School of Medicine, Kobe, Japan*

Correspondence
Ichiro Sora, Department of Psychiatry, Kobe University Graduate School of Medicine, 7-5-1 Kusunoki-cho, Chuo-ku, Kobe 650-0017, Japan. E-mail: sora@med.kobe-u.ac.jp

Received
24 September 2013
Revised
9 May 2014
Accepted
24 May 2014

BACKGROUND AND PURPOSE

μ Opioid receptor knockout (MOP-KO) mice display several behavioural differences from wild-type (WT) littermates including differential responses to nociceptive stimuli. Brain structural changes have been tied to behavioural alterations noted in transgenic mice with targeting of different genes. Hence, we assess the brain structure of MOP-KO mice.

EXPERIMENTAL APPROACH

Magnetic resonance imaging (MRI) voxel-based morphometry (VBM) and histological methods were used to identify structural differences between extensively backcrossed MOP-KO mice and WT mice.

KEY RESULTS

MOP-KO mice displayed robust increases in regional grey matter volume in olfactory bulb, several hypothalamic nuclei, periaqueductal grey (PAG) and several cerebellar areas, most confirmed by VBM analysis. The largest increases in grey matter volume were detected in the glomerular layer of the olfactory bulb, arcuate nucleus of hypothalamus, ventrolateral PAG (VLPAG) and cerebellar regions including paramedian and cerebellar lobules. Histological analyses confirm several of these results, with increased VLPAG cell numbers and increased thickness of the olfactory bulb granule cell layer and cerebellar molecular and granular cell layers.

CONCLUSIONS AND IMPLICATIONS

MOP deletion causes previously undescribed structural changes in specific brain regions, but not in all regions with high MOP receptor densities (e.g. thalamus, nucleus accumbens) or that exhibit adult neurogenesis (e.g. hippocampus). Volume differences in hypothalamus and PAG may reflect behavioural changes including hyperalgesia. Although the precise relationship between volume change and MOP receptor deletion was not determined from this study alone, these findings suggest that levels of MOP receptor expression may influence a broader range of neural structure and function in humans than previously supposed.

LINKED ARTICLES
This article is part of a themed section on Opioids: New Pathways to Functional Selectivity. To view the other articles in this section visit http://dx.doi.org/10.1111/bph.2015.172.issue-2

Abbreviations
DARTEL, diffeomorphic anatomical registration through exponentiated lie algebra; FWHM, full width at half maximum; GM, grey matter; MOP, μ opioid; MOP-KO, μ opioid receptor knockout; NPY, neuropeptide Y; PAG, periaqueductal grey; RARE, rapid acquisition with refocused echoes; ROI, region of interest; SNR, signal-to-noise ratio; VBM, voxel-based morphometry; VLPAG, ventrolateral PAG; WM, white matter; WT, wild type

Table of Links

TARGETS	LIGANDS
MOP, μ opioid receptor	β endorphin
	NPY, neuropeptide Y

This Table lists the protein targets and ligands in this article which are hyperlinked to corresponding entries in http://www.guidetopharmacology.org, the common portal for data from the IUPHAR/BPS Guide to PHARMACOLOGY (Pawson *et al.*, 2014) and the Concise Guide to PHARMACOLOGY 2013/14 (Alexander *et al.*, 2013).

Introduction

Studies in knockout mice have demonstrated that μ opioid (MOP) receptors play important roles in regulating several behavioural and physiological functions including nociception, reward, drug dependence, stress responses, immune function, aspects of brain development and feeding behaviour (Sora *et al.*, 1997a,b; 2001; Roy *et al.*, 1998; Fuchs *et al.*, 1999; Filliol *et al.*, 2000; LaBuda *et al.*, 2000a; Hall *et al.*, 2001; Zagon *et al.*, 2002; Ide *et al.*, 2004). Pain-related behaviours are among those most extensively examined in MOP receptor knockout (MOP-KO) mice (Sora *et al.*, 1997b; 2001; LaBuda *et al.*, 2000b).

MOP receptors are broadly and multifocally expressed in the dorsal horn of the spinal cord and in many supraspinal brain regions (Mansour *et al.*, 1987; Kitchen *et al.*, 1997). A number of studies have demonstrated the importance of several brain sites in modulating nociception and/or in mediating the analgesic effects of MOP receptor-induced antinociception, including the periaqueductal grey (PAG) (Lewis and Gebhart, 1977; Manning, 1998), thalamus (Cohen and Melzack, 1985; Yang *et al.*, 2002), hypothalamus and amygdala (Manning, 1998). PAG and hypothalamus have been identified as the primary brain sites of analgesic actions of MOP receptor agonists (Manning *et al.*, 1994). As a consequence of the development of MOP-KO mice, the neurobiological contributions of MOP receptor to a variety of physiological functions have been more fully elucidated (Sora *et al.*, 2003). This includes a demonstration by Eisch and colleagues of a role for MOP receptors in modulating adult neurogenesis (Harburg *et al.*, 2007). However, the relationship between MOP receptor gene deletion and brain structural changes has not been examined. Brains of several strains of mutant mice have been shown to exhibit structural changes, when examined carefully, in ways that can display correlations with behavioural consequences of genetic modifications (Nieman *et al.*, 2007). Structural changes in the brain are increasingly identified using magnetic resonance imaging (MRI) scans that sample the entire brain, supplemented by histological studies of specific brain regions (Ma *et al.*, 2005; Biedermann *et al.*, 2012). In order to investigate the brain structure of MOP-KO mice, we now report neuroimaging voxel-based morphometry (VBM) analyses followed by focal histological confirmatory studies. Several of the changes that we note in these brains can be related, at least tentatively, to behavioural alterations that we have previously reported in these mice.

Methods

Animals

All animal care and experimental procedures were approved by the Institutional Animal and Care Committee of Tohoku University. All studies involving animals are reported in accordance with the ARRIVE guidelines for reporting experiments involving animals (McGrath *et al.*, 2010; Kilkenny *et al.*, 2011). A total of 84 animals were used in the experiments described here.

Congenic homozygous MOP-KO mice and wild-type (WT) mice were used in these studies that had been backcrossed for at least 20 generations to C57BL/6J mice (Sora *et al.*, 1997a; Hall *et al.*, 2003). All mice were housed at the Institute for Animal Experimentation, Tohoku University Graduate School of Medicine, in a colony maintained at an ambient temperature of 22 ± 2°C, on a 12 h light:12 h dark cycle (lights on 08:00–20:00) with food and water available *ad libitum*. All mice were housed four to six per cage and were 12 weeks of age for both MRI scanning and histology. Forty-

two homozygous MOP-KO mice (30 ± 2.4 g; values are mean ± SD) and 42 WT mice (25.6 ± 1.6 g) were used for MRI imaging. For histological studies, seven mice for each genotype were used.

Image acquisition

Each mouse was anaesthetized with isoflurane (5% for initial induction and 2.0% during MRI scanning for maintenance) in a gas mixture of 40% O_2 and 60% N_2. Isoflurane was chosen because it has a negligible influence on tissue perfusion (Maekawa *et al.*, 1986). Each mouse was placed in the prone position on a custom-built MRI bed with a bite bar and a gas mask. Core body temperature was monitored throughout the MRI scan using an MRI-compatible temperature probe (model 1025; SA Instruments, Stony Brook, NY, USA) inserted into the rectum and regulated at 37.0 ± 1.0°C using a water-circulating pad. All MRI data were acquired using a 7.0-T Bruker PharmaScan System (Bruker Biospin, Ettlingen, Germany) with a 23 mm in diameter birdcage coil that was designed to image the mouse brain. Prior to the acquisition of MRI data, global magnetic field shimming was performed inside the core and at the region of interest (ROI) using a point-resolved spectroscopic protocol (Sumiyoshi *et al.*, 2011). The line width (full width at half maximum, FWHM) at the end of the shimming procedure ranged from 10 to 15 Hz in the ROI. The T1 tissue contrast between grey and white matter (WM) is less pronounced at a high magnetic field strength in rodents compared with humans (van de Ven *et al.*, 2007), presumably due to differences in cytoarchitecture (e.g. neuronal density) between these two species (DeFelipe *et al.*, 2002) as well as the distinct effects of anaesthesia (e.g. isoflurane) on tissue perfusion and metabolism of grey and WM (Maekawa *et al.*, 1986). Therefore, we used T2-weighted images in this study. T2-weighted images have been used in previous VBM (Sawiak *et al.*, 2009; Biedermann *et al.*, 2012) and deformation-based morphometry (Lerch *et al.*, 2011; Gaser *et al.*, 2012) studies in rodents. The T2-weighted images were obtained using the respiration-gated 2D-rapid acquisition with refocused echoes (RARE) sequence with the following parameters: repetition time = 4628 ms, effective echo time = 30 ms, RARE factor = 4, flip angle = 90 degrees, field of view = 18 × 18 mm^2, matrix size = 144 × 144, voxel size = 125 × 125 m^2, number of slices = 54, slice thickness = 300 μm and number of averages = 20. The total MRI scanning time for each mouse was approximately 60 min depending on the respiration rate. The MRI acquisition parameters were set to achieve a reasonable signal-to-noise ratio (SNR) of the T2-weighted images (Kale *et al.*, 2008) and to reduce the total exposure time to anaesthesia during the MRI acquisition. The SNR for each T2-weighted image was 39 ± 8 (mean ± SD), which was measured as the mean image intensity in a single slice of the brain divided by the standard deviation of the intensity in the background outside the brain.

Image preprocessing

The MRI image analysis was performed with the Statistical Parametric Mapping 8 (SPM8; Wellcome Trust Centre for Neuroimaging, London, UK) toolbox and custom-written software in MATLAB (MathWorks, Natick, MA, USA). First, each T2-weighted image was resized by a factor of 10 to account for the whole-brain volume difference between human and rodent (Biedermann *et al.*, 2012), and the rigid body was aligned to the stereotaxic space by registering each image to the template image, and was resampled into 700 μm isotropic voxels (for the resized images). Second, each image was segmented into probability maps of grey matter (GM), WM and CSF using the unified segmentation approach (Ashburner and Friston, 2005), which enables image registration, tissue classification and bias correction to be combined within the unified generative model. For the unified segmentation steps, the default settings in the SPM8 toolbox were used (e.g. warping regularization: 1; warp frequency cut-off: 25; bias regularization: 0.0001; bias FWHM: 60 mm cut-off; and sampling distance: 3), except that human tissue priors were replaced by mouse tissue priors (Sawiak *et al.*, 2009). Third, all of the individual segmented tissue maps (GM and WM maps) were used to create a customized and population-specific template using the DARTEL (diffeomorphic anatomical registration through exponentiated lie algebra) algorithm, which is an automated, unbiased and non-linear template building program (Ashburner, 2007). For the DARTEL template creation steps, the default settings in the SPM8 toolbox were used. Fourth, all of the individual GM maps were spatially normalized onto the population-specific template space. The signal intensity of the normalized maps was modulated by the determinant of the Jacobian of the transformation (Ashburner and Friston, 2000) to account for the expansion and/or contraction of brain regions. Fifth, the population GM template was rigid body aligned to the stereotaxic space through an affine transformation. Finally, all of the individual GM maps were co-registered to the stereotaxic atlas space using the same affine transformation and were smoothed with a 4 mm FWHM Gaussian kernel for the resized images. Although the image preprocessing was performed using resized scales, the results of the VBM analysis are displayed in the original scales. To compare the whole-brain volumes, the total amounts of GM, WM and CSF in the brain from the segmented tissue maps were summed to provide the total intracranial volume for each subject.

Data (image) analysis

We tested for group-wise differences in the GM maps across the whole brain using the voxel-by-voxel two-sample *t*-test based on the general linear model in the SPM8 toolbox. The age and sex of the subjects were identical; therefore, no age or sex factors confounded the statistical image analysis. We did observe significant differences in intracranial volume between groups (see 'Results' section). We thus included intracranial volume as a covariate in order to control for the effect of individual brain sizes, as is standard practice for VBM analysis (Ridgway *et al.*, 2008). We excluded all voxels with a GM value less than 0.2 by creating an exclusive mask based on the population-specific GM template to avoid possible edge effects around the borders between GM and WM and to include only voxels with sufficient GM proportions (May *et al.*, 2007). Statistically significant clusters were identified using a threshold of $P < 0.05$ (e.g. $t > 2.578$) after which a false discovery rate correction for multiple comparisons was

applied across all brain voxels (Genovese *et al.*, 2002). A cluster-extent threshold of $P < 0.01$ was also applied (Friston, 1996).

Histological analysis

After MRI image acquisition, each mouse was anaesthetized with a lethal dose of pentobarbital and perfused transcardially with cold 0.1 M PBS followed by 4% paraformaldehyde in 0.1 M PBS (pH 7.4) for 30 min at rate of 7 mL·min^{-1}. After perfusion, brains were removed and post-fixed in 4% paraformaldehyde in 0.1 M PBS. After post-fixation, tissues were embedded in paraffin using a specialized automated tissue processing system (SAKURA Tissue-Tek, Sakura Finetek Japan Co., Ltd., Tokyo, Japan) at 58°C. Three micrometer coronal sections were taken through the olfactory bulb (bregma 3.5 mm), hypothalamus (bregma –1.65 mm), PAG (bregma –4.5 mm) and cerebellum (bregma –6 mm) for each MOP-KO and WT mouse (Paxinos and Franklin, 2004). Alternate sections were used for haematoxylin and eosin (H&E) and Klüver-Barrera (KB) staining. H&E staining procedures were as follows: deparaffinize sections in xylene, 10–20 min; rehydrate sections: 100% alcohol for 1–2 min, 95% alcohol for 1–2 min; rinse in tap water and distilled water; stain with haematoxylin (Chroma, Köngen, Germany) for 25 min; wash in tap water; differentiate section with 1% HCl in 70% alcohol, 1–2 dips and check under microscope; if necessary, return slides to HCl for further differentiation; wash slides in running tap water for 15 min; dip slides in 95% alcohol; stain slides in eosin (Merck, Darmstadt, Germany) for 2 min; dehydrate and differentiate using 95% alcohol, 5–6 dips and 100% alcohol, 5–6 dips; clear slides in xylene two times; mount slides with mounting media. KB staining procedures are as follows: deparaffinize and hydrate to 95% alcohol; 0.1% Luxol fast blue (Sigma-Aldrich Japan, Tokyo, Japan) solution at 56–60°C overnight; rinse in 95% alcohol to remove excess stain and distilled water; after removing excess stain, begin differentiation by quick immersion in 0.05% lithium carbonate solution; continue differentiation in 70% alcohol solution until grey and WM can be distinguished and wash in distilled water; final differentiation by rinsing briefly in lithium carbonate solution and then putting through several changes of 70% alcohol until the greenish blue of the WM contrasts sharply with the colourless GM and rinse thoroughly in distilled water; 0.1% cresyl violet solution (Sigma-Aldrich Japan) for 6 min (filter and preheat cresyl violet to 57°C just before use); differentiate in several changes of 95% alcohol (add a few drops of 5N HCL to speed differentiation); dehydrate in absolute alcohol; and clear in xylene. The number of nuclei (neurons, glia and endothelial cells) was counted using an automated cell counting microscope, KEYENCE BZ-9000 (KEYENCE, Tokyo, Japan), and a *t*-test was used to compare genotypes. Neuronal profile areas were measured on H&E sections through the ventrolateral PAG (VLPAG; 641 × 475 pixels) and the arcuate nucleus of the hypothalamus (951 × 688 pixels) under low magnification (×40), following standard mouse brain coordinates (Paxinos and Franklin, 2004). In the olfactory bulb, the width of the glomerular and granule cell layers was measured at five different points in five sections for each genotype ($n = 7$). In the cerebellum, the widths of the molecular and granule cell layers were measured in a similar manner. Width measurements were also performed by KEYENCE BZ-9000 (KEYENCE), and a *t*-test was used to compare these values between genotypes.

Results

Neuroimaging analysis

VBM detected relatively robust volume differences between MOP-KO and WT mice. MOP-KO mice exhibited increased regional GM volume ($P < 0.01$) and increased intracranial volume ($P < 0.001$) compared with WT mice (Table 1).

Coronal slices throughout the brain, presented in a caudal to rostral series (Figure 1), illustrated the corresponding significant differences in the GM volume between the MOP-KO mice and WT mice. MOP-KO mice exhibited significantly increased GM volumes in several specific brain regions. These regions included olfactory bulb, hypothalamus, PAG and specific cerebellar regions. The statistically significant regions of increased GM volume were identified using a threshold of $P < 0.05$ (corresponding to $t > 2.578$).

The neuroimaging picture and anatomical locations of the most significantly increased regional GM volume changes in the MOP-KO mice compared with WT mice are presented in Figure 2 and Table 2. The greatest increases in regional GM volumes in MOP-KO mice were found in the glomerular layer of olfactory bulb (Figure 2, panels 1-A, B), arcuate nucleus of the hypothalamus (Figure 2, panels 2-A, B), VLPAG (Figure 2, panels 3-A, B), copula of the pyramis of the cerebellum (Figure 2, panel 4-A), cerebellar lobule of the cerebellum (Figure 2, panel 4-B) and paramedian lobule of the cerebellum (Figure 2, panel 4-C). Statistically significant regions of increased GM volume in these structures were identified using a threshold of $t > 2.578$ (corresponding to $P < 0.05$).

Histology

Confirmatory histological analyses were performed for the glomerular layer of the olfactory bulb, arcuate nucleus of the hypothalamus, VLPAG, copula of the pyramis of the cerebellum, cerebellar lobule of the cerebellum and paramedian lobule of the cerebellum. Representative photomicrographs for the glomerular layer of the olfactory bulb are presented in Figure 3. Under the lower magnification overall architecture of olfactory bulb was very similar between genotypes (Figure 3, panels A-1, A-2 and B-1, B-2). Under higher magnification, there was no evidence for neuronal or glial

Table 1

Intracranial and grey matter volume in MOP-KO and WT mice

	WT	MOP-KO
Intracranial volume (ICV)	501.9 ± 23.2	521.9 ± 25.8***
Grey matter volume (GM)	281.2 ± 8.0	288.3 ± 10.7**

Average volume of grey matter and whole brain (intracranial) was measured in MOP-KO mice ($n = 42$) and WT mice ($n = 42$). **$P < 0.01$ ***$P < 0.001$ significant difference from corresponding value in WT mice. Values are expressed as means ± SD.

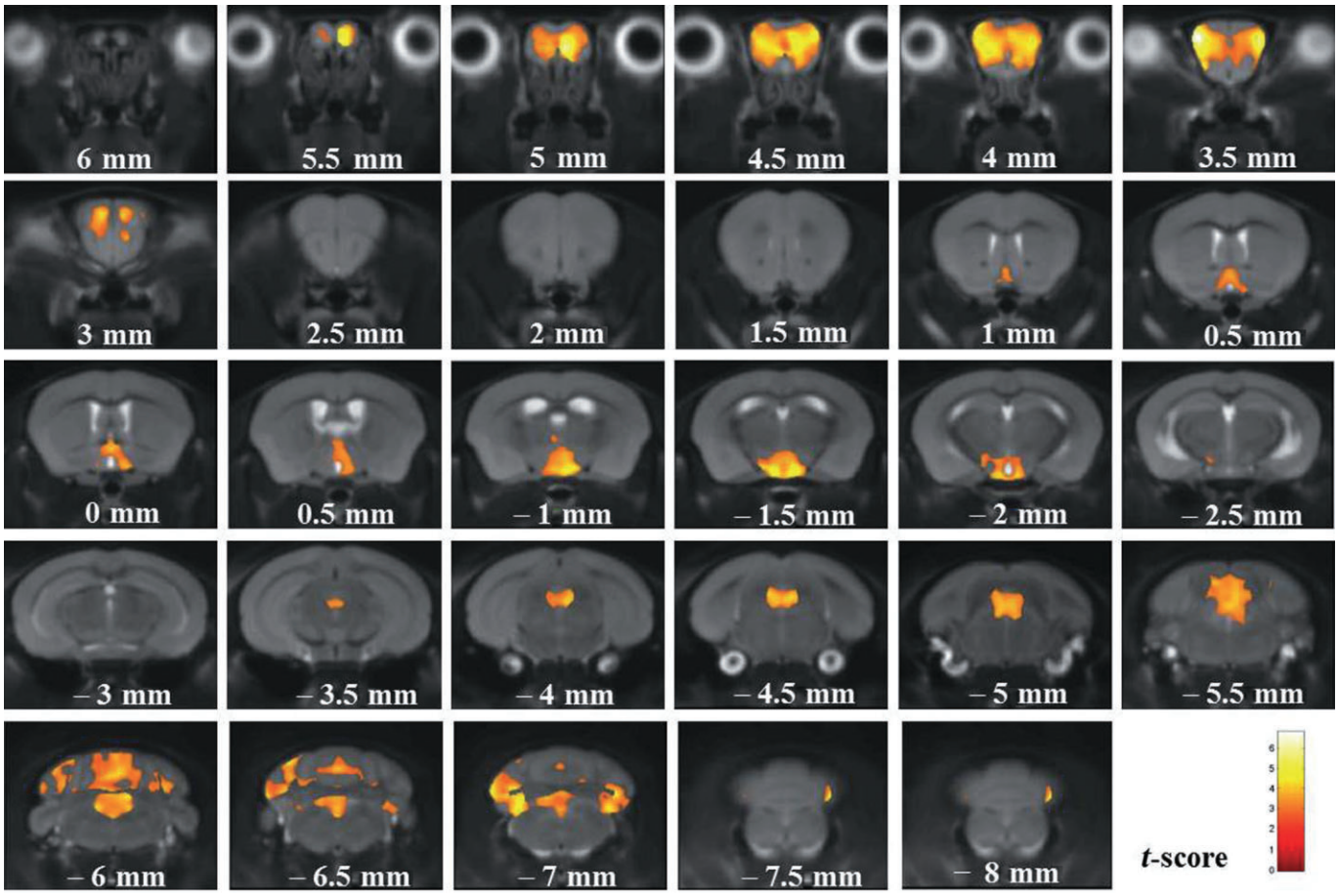

Figure 1

Coronal view of areas demonstrating significant increase in regional grey matter volume in MOP-KO mice. Results of VBM analysis. $t > 2.578$ ($P < 0.05$), significant increases in regional grey matter volume in MOP-KO mice. Colour bar units represent *t*-values.

pathological degeneration (Figure 3, panels A-3, A-4 and B-3, B-4).

Data from the olfactory bulb measurements are presented in Table 3. The thickness of the glomerular layer in knockout mice did not differ from that seen in WT mice. However, there was increased granule cell layer thickness in MOP-KO mice ($P < 0.05$) that could contribute to the overall volumetric differences noted in VBM studies.

Representative photomicrographs of the arcuate nucleus of the hypothalamus are presented in Figure 4. Under the lower magnification the overall architecture of this region was similar between genotypes (Figure 4, panels C-1, C-2 and D-1, D-2). Higher magnification revealed no evidence for chromatolysis, ischaemic cell change, vacuolar degeneration, deposits or myelin degeneration in either MOP-KO or WT mice (Figure 4, panels C-3, C-4 and D-3, D-4).

Automated cell counts did not identify significant differences in cell numbers in the arcuate nucleus (Table 4).

Representative photo micrographs of VLPAG are presented in Figure 5. Under lower magnification, the overall architecture of this region did not appear to differ between genotypes (Figure 5, panels E-1, E-2 and F-1, F-2). Under higher magnification, there was no evidence for neuronal or glial pathological degeneration (Figure 5, panels E-3, E-4 and F-3, F-4). Automated cell counts in VLPAG did reveal increased numbers of cells, including neurons, glia and endothelial cells, in MOP-KO mice compared with WT mice ($P < 0.05$).

Overall morphology of molecular and granule cell layers in the cerebellum did differ between MOP-KO and WT mice (Figure 6, panels G-1, G-2 and H-1, H-2). There was increased molecular and granule cell layer thickness in MOP-KO mice ($P < 0.001$; Table 5). There was no evidence for pathological degeneration in MOP-KO mice (Figure 6, panels G-3, G-4 and H-3, H-4).

Discussion

The findings of this study focus on the remarkable increases in grey matter and intracranial volumes identified in MOP-KO mice, with especial prominence in nervous system regions that include olfactory bulb, hypothalamus, PAG and cerebellum. Furthermore, in several of these regions, there was supporting histological evidence for increased numbers of cells and/or increased thickness of specific cell layers. In

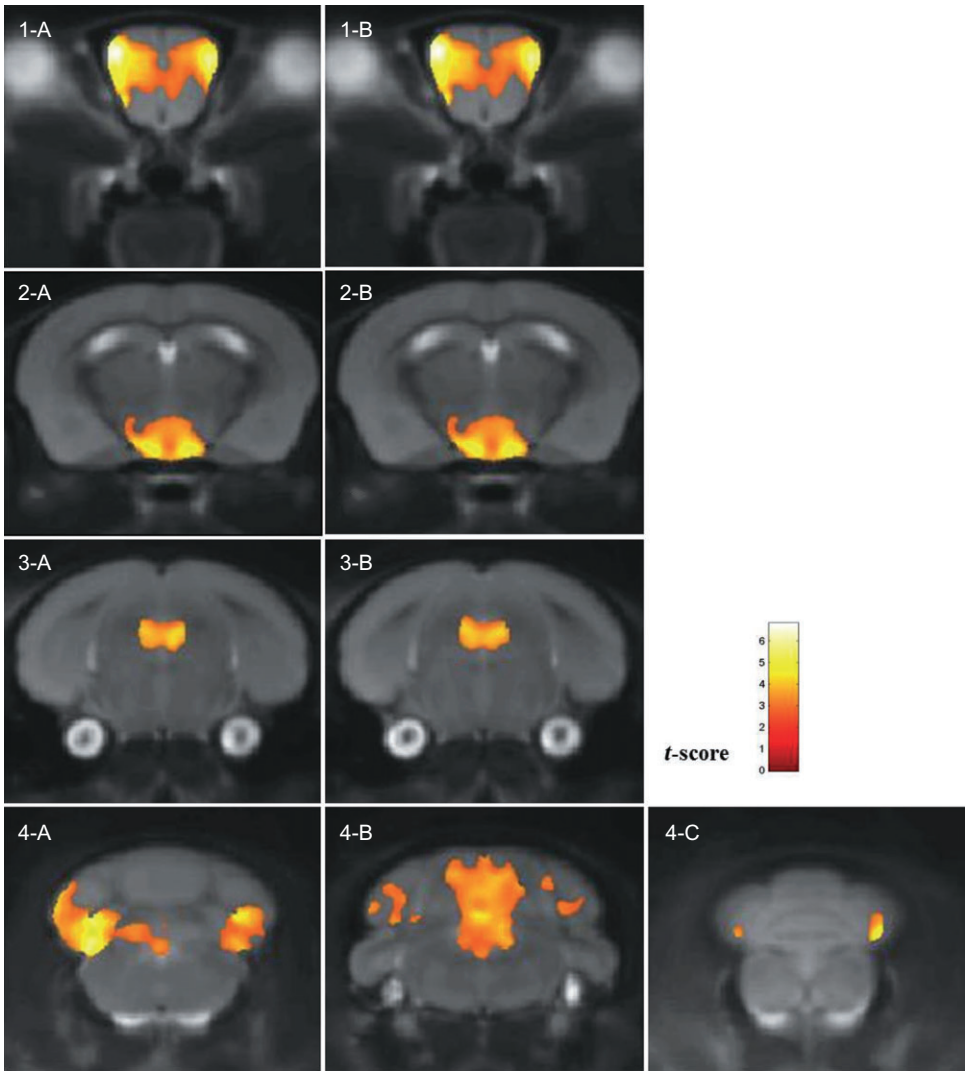

Figure 2

Regional increases in regional grey matter volume in MOP-KO mice in the olfactory bulb, hypothalamus, PAG and cerebellum. Significant increases in regional grey matter volume in MOP-KO mice. Olfactory bulb (panel 1-A, B), hypothalamus (panels 2-A, B), PAG (panels 3-A, B) and cerebellum (panels 4-A–C). The location from bregma is described in Table 2. $t > 2.578$ ($P < 0.05$), significant increases in regional grey matter volume in MOP-KO mice. Colour bar units represent *t*-values.

the present study there was no clear detection of neural, glial or endothelial cell types that might possibly contribute to increased cell numbers in specific brain regions of MOP-KO mice. Further analysis and detection of these specific cell types by immunological staining will be required in future studies to specify the cell type-specific changes in MOP-KO mice. In the present study, examination under optical microscope of H&E and KB stained sections revealed no degenerative histological evidence in MOP-KO mice. However, as we did not examine specific markers for degeneration, such as caspase or TUNEL that can detect apoptosis, these conclusions need to be qualified to some degree.

This remarkable and novel pattern of brain and regional brain volume changes in MOP-KO mice can be considered in terms of the relationships between the altered regions and MOP receptor expression, the behavioural features that might provide correlates of these regional differences, the developmental mechanisms that might be involved and the implications of these observations for MOP receptor-based therapeutics and illicit substances.

It is possible to link several of these regional brain volume differences to differences in nociceptive and analgesic properties that have been previously reported in MOP-KO mice (Sora *et al.*, 1997b; LaBuda *et al.*, 2000b). A current anatomical model of the PAG proposes an organization into four parallel longitudinal columns: the dorsomedial, dorsolateral, lateral and ventrolateral (VLPAG), each with distinct physiological functions (Bandler *et al.*, 2000; Linnman *et al.*, 2012). Opioid-mediated analgesia is believed to involve VLPAG (Bandler and Shipley, 1994). Histological identification of increased number of neurons, glia and endothelial cells in VLPAG provides a structural underpinning for at least a part

Table 2

Anatomical regions with significant volume changes in VBM analysis

Region	Bregma Lateral	Bregma Ventral	Bregma Anterior	*t*-value
Cerebellum (paramedian lobule)	–2.57	4.33	–7.25	5.74
Cerebellum (cerebellar lobule)	–0.26	3.15	–5.78	4.51
Periaqueductal grey (VLPAG)	0.44	2.59	–4.38	4.23
Periaqueductal grey (VLPAG)	–0.68	2.52	–4.52	4.11
Olfactory bulb (glomerular layer)	–1.73	1.05	3.46	6.81
Olfactory bulb (glomerular layer)	1.49	1.33	3.46	6.01
Hypothalamus (arcuate nucleus)	0.51	5.52	–1.65	5.06
Hypothalamus (arcuate nucleus)	–0.61	5.52	–1.65	5.03
Cerebellum (copula of pyramis)	2.33	3.70	–7.95	5.01

The anatomical regions are indicated in terms of the distance from bregma (lateral, ventral, anterior) according to standard coordinates (Paxinos and Franklin, 2004). If specific structures are not listed, they contained no significantly different clusters. $t > 2.578$ ($P < 0.05$), significant difference from WT mice. MOP-KO mice ($n = 42$), WT mice ($n = 42$).

Table 3

Thickness of glomerular and granule cell layers of the olfactory bulb

	WT	MOP-KO
Glomerular layer (pixels)	18.7 ± 3.8	20.9 ± 4.6
Granule cell layer (pixels)	121.8 ± 17.9	138.9 ± 36.1*

The thicknesses of the glomerular and granule cell layers in the olfactory bulb were measured under low magnification (×40) in HE stained sections. The number of sections that were measured in this analysis was 25 for each genotype ($n = 5$). Measurements were carried out in five points in each region in one section. Thickness measurements are expressed in terms of number of pixels. *$P < 0.05$ significant difference from corresponding value in WT mice. Values are expressed as means ± SD.

Table 4

Cell numbers in VLPAG and arcuate nucleus of the hypothalamus

	WT	MOP-KO
VLPAG	216.0 ± 42.3	254.8 ± 46.1*
Arcuate nucleus	331.7 ± 53.0	316.8 ± 42.2

The numbers of nuclei were counted by an automated cell counting system (BZ-9000, KEYENCE) in VLPAG (641 × 475 pixels) and arcuate nucleus of the hypothalamus (951 × 688 pixels) in each genotype under low magnification (×40) in HE stained sections. The number of sections that were measured in this analysis were 35 for each genotype ($n = 7$). *$P < 0.05$ significant difference from corresponding value in WT mice. Values are expressed as means ± SD.

Table 5

Thickness of molecular and granule layers of the cerebellum

	WT	MOP-KO
Molecular layer (pixels)	89.3 ± 10.2	327 ± 10.1***
Granule layer (pixels)	15.3 ± 3.1	31.3 ± 7.01***

The thicknesses of the molecular and granule cell layers in the cerebellum were measured under low magnification (×10) in HE stained sections. The number of sections measured in this analysis was 25 for each genotype. Measurement was made at five points in each region in one section. Thickness measurements are expressed in terms of number of pixels. ***$P < 0.001$ significant difference from corresponding value in WT mice. Values are expressed as means ± SD.

of the difference in regional volume in this PAG subregion that is implicated in opiate-mediated behaviour. These VLPAG differences appear likely to underlie some of the alterations in responses to thermal stimuli and stress-induced analgesia that have been previously reported in MOP-KO mice (Sora *et al.*, 1997b; LaBuda *et al.*, 2000b). In this previous work, MOP-KO mice displayed shorter latencies in tail flick and hot plate tests for spinal and supraspinal nociceptive responses than WT mice, for example (Sora *et al.*, 1997b). The arcuate nucleus of hypothalamus contributes to modulation of stress-induced analgesia by mechanisms that include release of β-endorphin (Frederickson and Geary, 1982; Sun *et al.*, 2003). Neurons from the arcuate project to the PAG and, in response to stressors, release the MOP receptor ligand β-endorphin. There are thus likely to be interactions between these two brain structures in stress-induced alterations in nociception (Mason, 2005). The observed volume changes in the arcuate nucleus could also have other implications as this region also plays important roles in appetite regulation and energy balance (Wang *et al.*, 2012). Although altered appetite

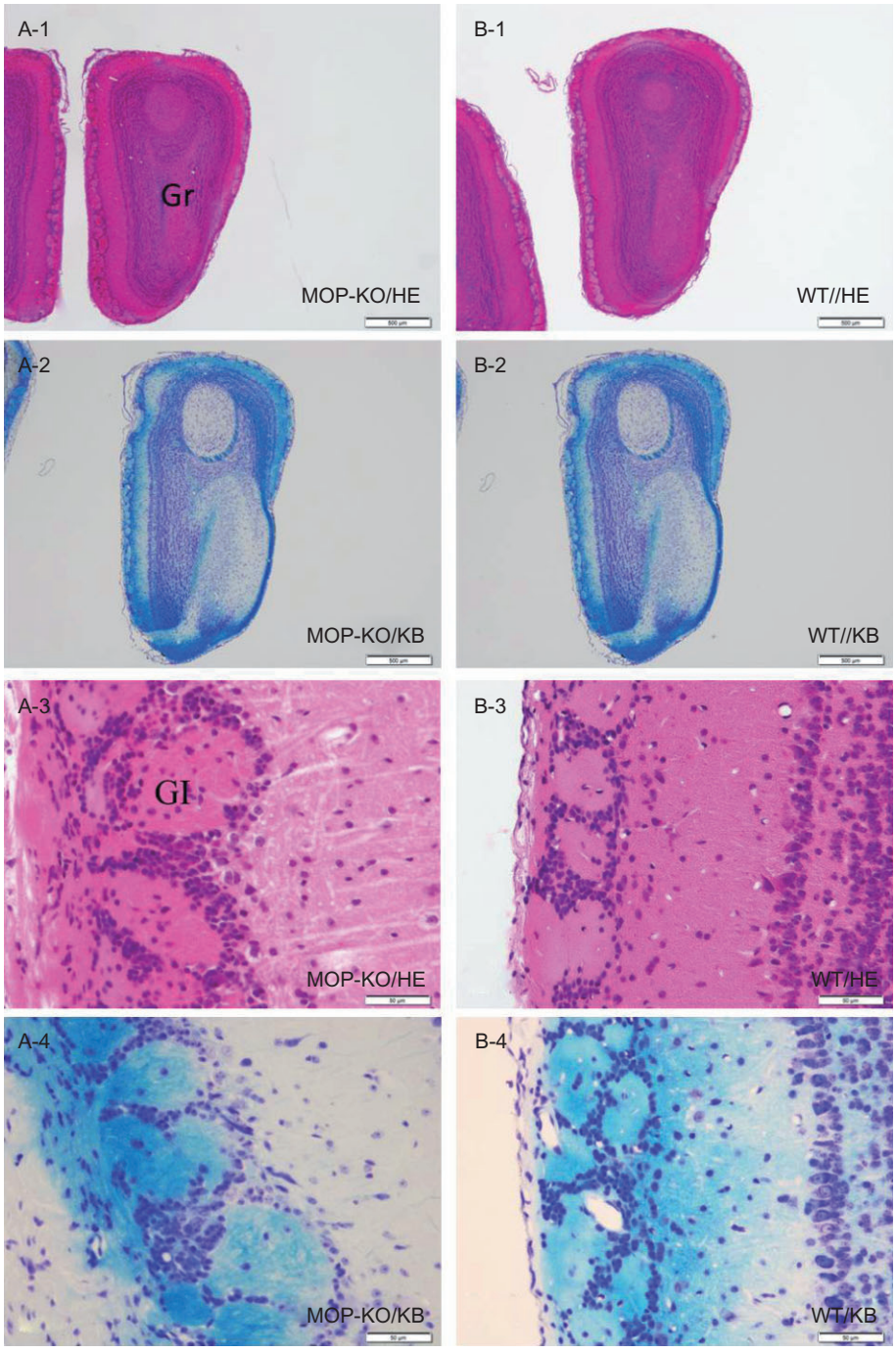

Figure 3

Representative photomicrographs of olfactory bulb. Histological features of olfactory bulb. (A-1, A-3), H&E staining in MOP-KO mice; (A-2, A-4), KB staining in MOP-KO mice; (B-1, B-3), H&E staining in WT mice; (B-2, B-4), KB staining in WT mice. Thickness was measured in the glomerular and granule cell layers of the olfactory bulb under the same magnification as sections A-1 and B-1. Measurements were performed at five different points in each region/section. GI, glomerular layer, Gr, granule cell layer. Scale bar indicates 500 µmm (A-1,2, B-1,2), 50 µmm (A-3,4, B-3,4).

has not been reported in MOP-KO mice, these mice do display up-regulated arcuate expression of mRNA encoding the feeding-related neuropeptide Y (NPY; Schwartz *et al.*, 2000; Han *et al.*, 2006). Conceivably, increased spine and/or neuropil density related to this up-regulated NPY expression could contribute to the observed volume change.

A number of developmental mechanisms might be involved in these regionally specific structural changes. Adult neurogenesis in the hippocampus has been well documented to be modulated by opiate agonists and to differ in MOP-KO mice (Eisch *et al.*, 2000; Harburg *et al.*, 2007). New neurons continue to migrate into the olfactory bulb throughout adult-

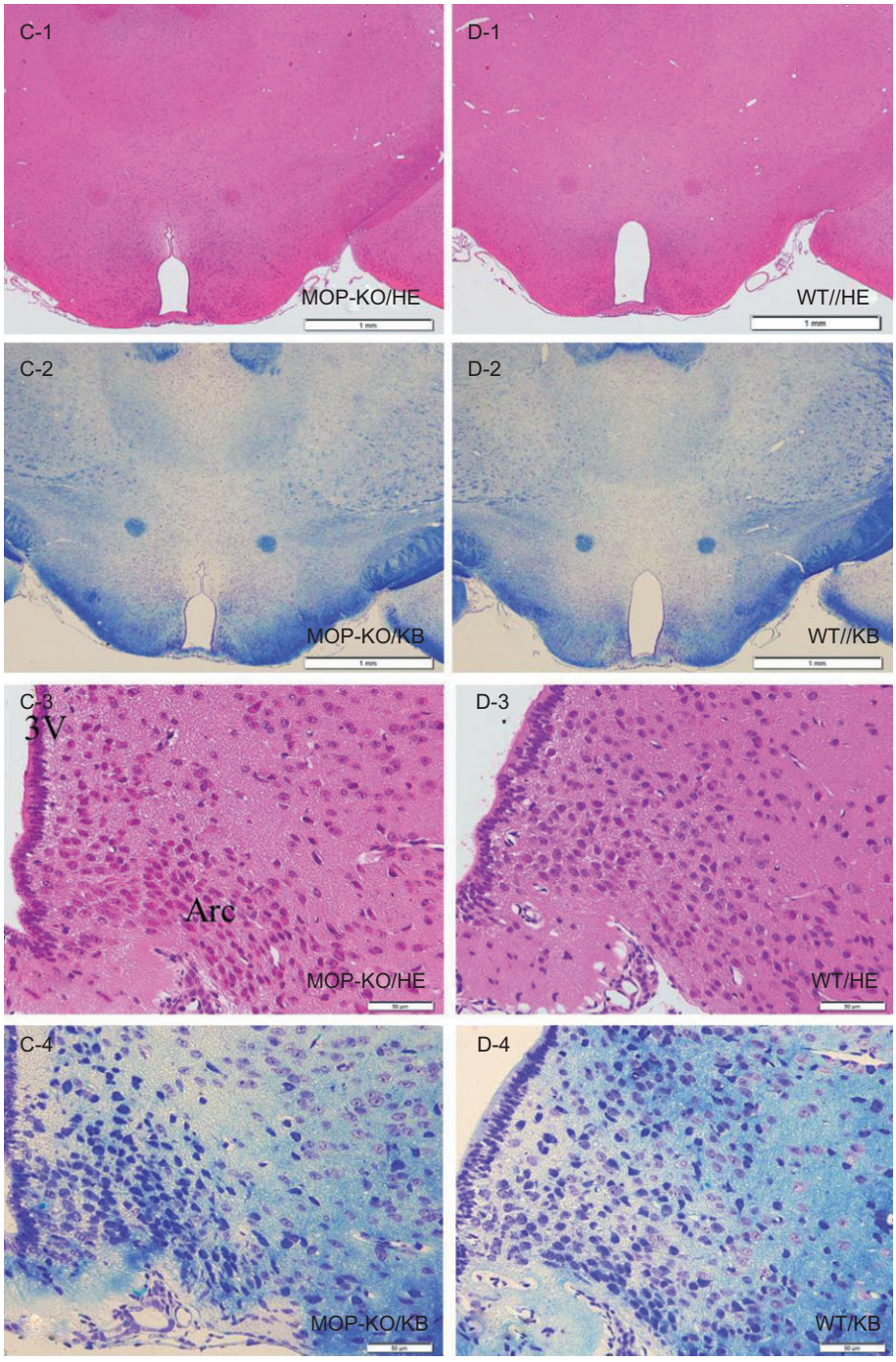

Figure 4

Representative photomicrographs of hypothalamus. Histological features of hypothalamus. (C-1, C-3), H&E staining in MOP-KO mice; (C-2, C-4), KB staining in MOP-KO mice; (D-1, D-3), H&E staining in WT mice; (D-2, D-4), KB staining in WT mice. Cell counting was performed in the arcuate nucleus of the hypothalamus (951 × 688 pixels) under the same magnification as in sections C-3 and D-3. Arc, arcuate nucleus of the hypothalamus; 3V, third ventricle. Scale bar indicates 1 mm (C-1,2, D-1,2), 50 µmm (C-3,4, D-3,4).

hood (Lledo *et al.*, 2006; Imayoshi *et al.*, 2009). Neuronal precursors generated in the subventricular zone (SVZ) migrate along the rostral migratory stream (RMS) into the olfactory bulb, where they differentiate into granular and periglomerular neurons, and integrate into established neuronal networks and respond to odour stimulation (Lledo and Saghatelyan, 2005). In rats, reduced volume of olfactory bulb in response to chronic stress exposure suggests that neurogenesis in the olfactory bulb may affect brain volume in this region (Yang *et al.*, 2011). The large stream of newborn neurons that

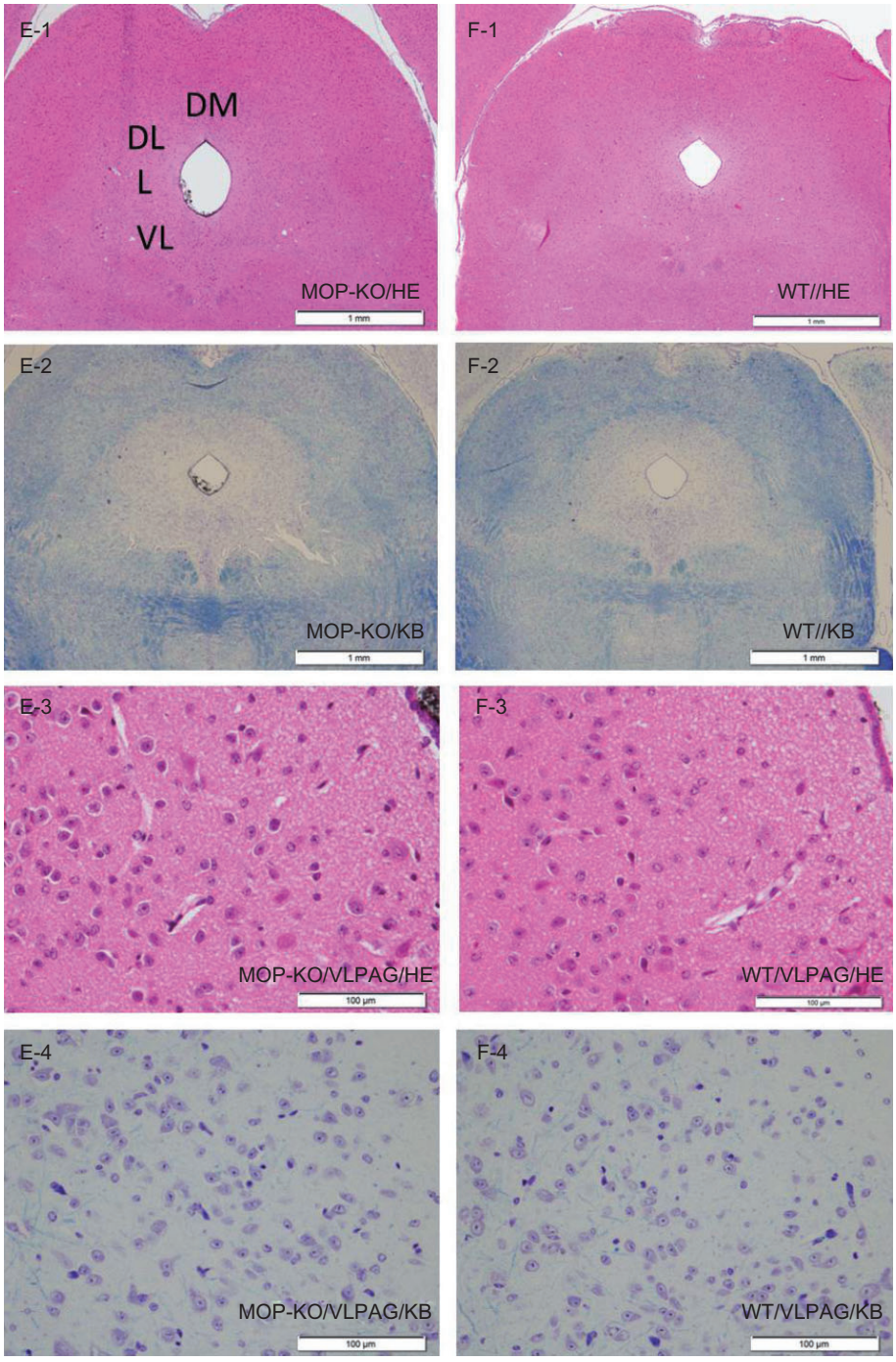

Figure 5

Representative photomicrographs of PAG. Histological features of PAG. (E-1, E-3), H&E staining in MOP-KO mice; (E-2, E-4), KB staining in MOP-KO mice; (F-1, F-3), H&E staining in WT mice; (F-2, F-4), KB staining in WT mice. Cell counting was performed in VLPAG (641 × 475 pixels) under the same magnification as sections E-3 and F-3. DL, dorsolateral; DM, dorsomedial; L, lateral; VL, ventrolateral. Scale bar indicates 1 mm (E-1,2, F-1,2), 100 μmm (E-3,4, F-3,4).

migrate to the olfactory bulb make such differences in neurogenesis strong candidates to play roles in the volumetric changes noted in this region. Differences in hypothalamic adult neurogenesis may also be involved, as recent evidence suggests that newborn cells are generated in the hypothalamic parenchyma, arcuate nuclei, ventromedial nuclei and dorsomedial nuclei (Cheng, 2013). However, another prominent region that is well documented to receive products of adult neurogenesis, the hippocampus, does not display volume differences between MOP-KO and WT mice.

Previous studies demonstrated that adult hippocampal neurogenesis in the MOP-KO mice is increased (Harburg

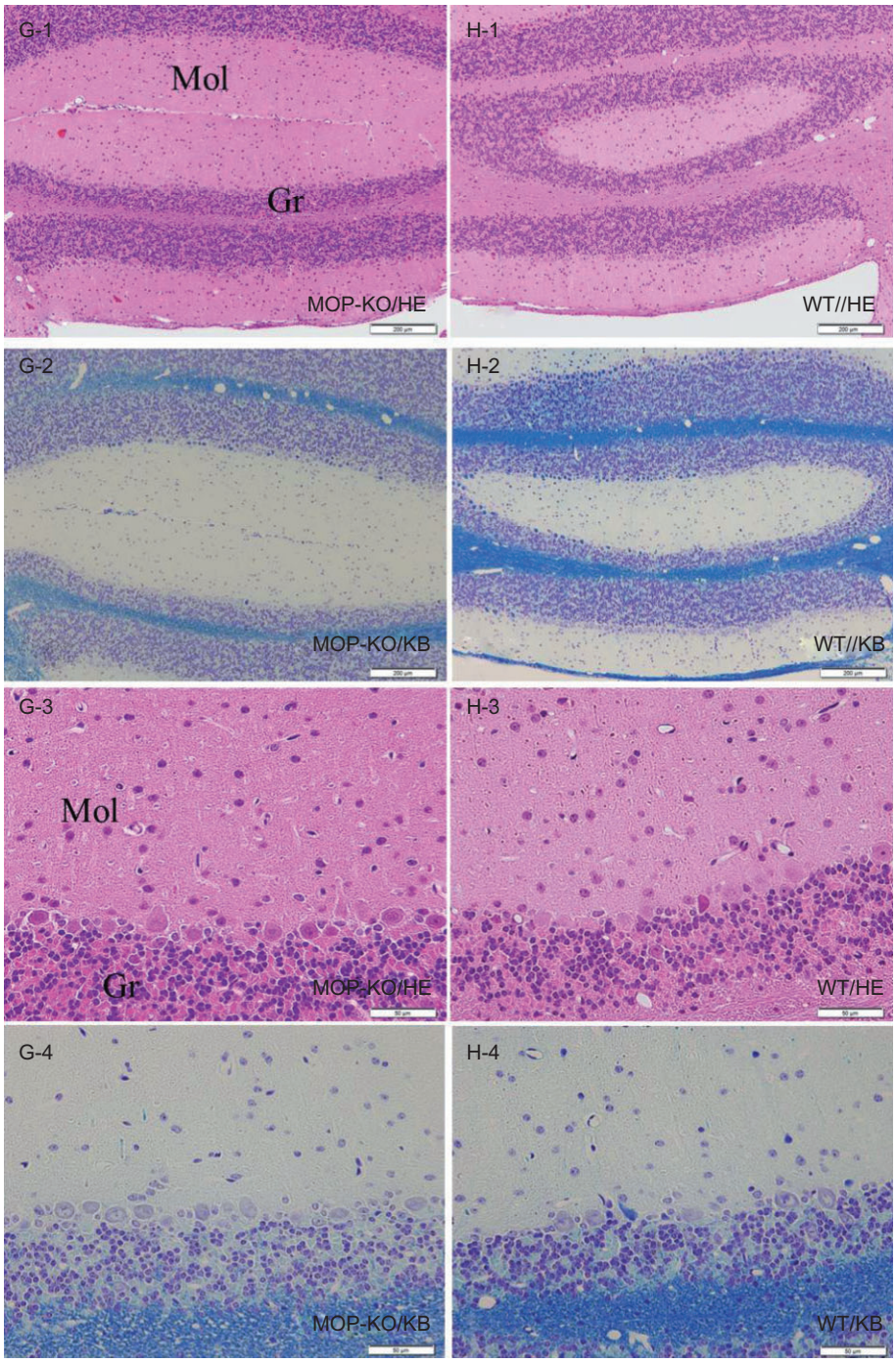

Figure 6

Representative photomicrographs of cerebellum. Histological features of cerebellum. (G-1, G-3), H&E staining in MOP-KO mice; (G-2, G-4), KB staining in MOP-KO mice; (H-1, H-3), H&E staining in WT mice; (H-2, H-4), KB staining in WT mice. Thickness was measured in the molecular and granule cell layers of the cerebellum under the same magnification as sections G-1 and H-1. Measurements were performed at five different points in each region/section. Gr, granule cell layer; Mol, molecular layer. Scale bar indicates 200 μm (G-1,2, H-1,2), 50 μmm (G-3,4, H-3,4).

et al., 2007; Cominski *et al.*, 2012). Although VBM and histological analysis in this study revealed increased brain volume in some specific brain regions in MOP-KO mice, no changes were observed in the hippocampus as might be suggested by these studies of hippocampal neurogenesis. Although we speculated that neurogenesis is one of the possible factors underlying differences in regional GM volume differences in some brain regions in this study, the results of hippocampal volume analysis by VBM were not predicted by the increased neurogenesis that has been observed in this region. At

present, we cannot conclude that there is a simple relationship between brain volume changes as determined in VBM analysis and neurogenesis. The specific cytological changes contributing to these volume changes in MOP-KO mice could not be determined in the present experiments, but it is also likely that these changes are not the result of changes in cell number alone.

Changes in spine and synapse densities alter neuropil volumes, provide one of the most prominent contributors to plasticity in most GM regions (Anderson, 2011). Variation in spine volume can change volume in several brain regions, including hypothalamus (Yuste and Bonhoeffer, 2001). The substantial adult expression of MOP receptors in most of the brain regions in which volumes differ in MOP-KO mice is consistent with large contributions of differences in neuropil to several of the brain volume differences noted here, although we have documented changes in numbers of cell bodies in some regions, such as VLPAG, as well.

It is also possible that developmental differences that alter neuropil and cell numbers might play roles in regions that include the cerebellum. Relatively high levels of MOP receptor-binding sites are present in cerebellum during early postnatal maturation (Zagon *et al.*, 1992), although opioid receptor mRNA and protein are sparse in mature cerebellum (Mansour *et al.*, 1994). The cerebellum in infant rats treated with the opioid antagonist naltrexone exhibits increased volume, including increased numbers of glial and granule cells (Zagon and McLaughlin, 1983). Although no clear-cut cerebellar phenotypes have been identified in MOP-KO mice, these pharmacological data are consistent with the magnitude and direction of the effects in MOP-KO mice that were found in the present study.

The present results add to data from pharmacological experiments that suggest caution in the use of MOP receptor-based therapeutic and illicit substances during development. Cellular brain adaptations to altered opioidergic signalling could be involved not only in neonatal abstinence syndromes and other readily observed sequelae of maternal opiate use in offspring, but might also lead to the brain regional differences in volume and function noted in children of opiate-addicted mothers. Although examination of conditional and regional selective knockout mice will be necessary to further elucidate critical periods and other details of the effects of MOP receptor deletion, the current findings add to the list of adaptations likely to follow prolonged use of opiate agonists or antagonists, especially during pregnancy.

Conclusion

This study detected brain volume abnormalities in MOP-KO mice. Hypothalamus and PAG, in which regionally specific changes were detected in MOP-KO mice, are important regions for MOP receptor-regulated physiological functions such as pain modulation, including stress-induced analgesia, and appetite modulation. This analysis may contribute to further understanding of the relationships between pathological degeneration in the hypothalamus and the PAG, behavioural alterations caused by MOP receptor deletion, and the effects of opiate agonists and antagonists on specific developmental processes.

Acknowledgements

This work was supported by a grant from Grants-in-Aid from MECSST and Health Sciences Research Grants from MHLW, Japan, and the Global COE Program, MEXT, Japan. This work was also supported in part by funding from the Intramural Research Program of the National Institute on Drug Abuse, USA (FSH, GRU). The authors would like to thank all of our colleagues at Tohoku University for their tremendous support.

Author contributions

I. S., K. S. and Y. K. were responsible for the conception and design of the study. A. S. and K. S. performed MRI analysis and interpretation of data. K. S. and H. N. conducted MRI data collection and assembly. K. S. was responsible for histological data collection and assembly. K. S. and M. W. performed histological analysis and interpretation of data. K. S. drafted the article. K. S., I. S., K. I., F. S. H., G. R. U. and R. K. conducted the critical revision of the article for important intellectual content. I. S. was responsible for the final approval of the article.

Conflict of interest

The authors declare no conflict of interest.

References

Alexander SPH, Benson HE, Faccenda E, Pawson AJ, Sharman JL Spedding M *et al* (2013). The Concise Guide to PHARMACOLOGY 2013/14: G Protein-Coupled Receptors. Br J Pharmacol 170: 1459–1581

Anderson BJ (2011). Plasticity of gray matter volume: the cellular and synaptic plasticity that underlies volumetric change. Dev Psychobiol 53: 456–465.

Ashburner J (2007). A fast diffeomorphic image registration algorithm. Neuroimage 38: 95–113.

Ashburner J, Friston KJ (2000). Voxel-based morphometry – the methods. Neuroimage 11 (6 Pt 1): 805–821.

Ashburner J, Friston KJ (2005). Unified segmentation. Neuroimage 26: 839–851.

Bandler R, Shipley MT (1994). Columnar organization in the midbrain periaqueductal gray: modules for emotional expression? Trends Neurosci 17: 379–389.

Bandler R, Keay KA, Floyd N, Price J (2000). Central circuits mediating patterned autonomic activity during active vs. passive emotional coping. Brain Res Bull 53: 95–104.

Biedermann S, Fuss J, Zheng L, Sartorius A, Falfan-Melgoza C, Demirakca T *et al.* (2012). In vivo voxel based morphometry: detection of increased hippocampal volume and decreased glutamate levels in exercising mice. Neuroimage 61: 1206–1212.

Cheng MF (2013). Hypothalamic neurogenesis in the adult brain. Front Neuroendocrinol 34: 161–178.

Cohen SR, Melzack R (1985). Morphine injected into the habenula and dorsal posteromedial thalamus produces analgesia in the formalin test. Brain Res 359: 131–139.

Cominski TP, Turchin CE, Hsu MS, Ansonoff MA, Pintar JE (2012). Loss of the mu opioid receptor on different genetic backgrounds leads to increased bromodeoxyuridine labeling in the dentate gyrus only after repeated injection. Neuroscience 206: 49–59.

DeFelipe J, Alonso-Nanclares L, Arellano JI (2002). Microstructure of the neocortex: comparative aspects. J Neurocytol 31: 299–316.

Eisch AJ, Barrot M, Schad CA, Self DW, Nestler EJ (2000). Opiates inhibit neurogenesis in the adult rat hippocampus. Proc Natl Acad Sci U S A 97: 7579–7584.

Filliol D, Ghozland S, Chluba J, Martin M, Matthes HW, Simonin F *et al*. (2000). Mice deficient for delta- and mu-opioid receptors exhibit opposing alterations of emotional responses. Nat Genet 25: 195–200.

Frederickson RC, Geary LE (1982). Endogenous opioid peptides: review of physiological, pharmacological and clinical aspects. Prog Neurobiol 19: 19–69.

Friston KJ (1996). Statistical Parametric Mapping and Other Analyses of Functional Imaging Data. Academic Press: New York.

Fuchs PN, Roza C, Sora I, Uhl G, Raja SN (1999). Characterization of mechanical withdrawal responses and effects of mu-, delta- and kappa-opioid agonists in normal and mu-opioid receptor knockout mice. Brain Res 821: 480–486.

Gaser C, Schmidt S, Metzler M, Herrmann KH, Krumbein I, Reichenbach JR *et al*. (2012). Deformation-based brain morphometry in rats. Neuroimage 63: 47–53.

Genovese CR, Lazar NA, Nichols T (2002). Thresholding of statistical maps in functional neuroimaging using the false discovery rate. Neuroimage 15: 870–878.

Hall FS, Sora I, Uhl GR (2001). Ethanol consumption and reward are decreased in mu-opiate receptor knockout mice. Psychopharmacology (Berl) 154: 43–49.

Hall FS, Li XF, Goeb M, Roff S, Hoggatt H, Sora I *et al*. (2003). Congenic C57BL/6 mu opiate receptor (MOR) knockout mice: baseline and opiate effects. Genes Brain Behav 2: 114–121.

Han W, Hata H, Imbe H, Liu QR, Takamatsu Y, Koizumi M *et al*. (2006). Increased body weight in mice lacking mu-opioid receptors. Neuroreport 17: 941–944.

Harburg GC, Hall FS, Harrist AV, Sora I, Uhl GR, Eisch AJ (2007). Knockout of the mu opioid receptor enhances the survival of adult-generated hippocampal granule cell neurons. Neuroscience 144: 77–87.

Ide S, Minami M, Satoh M, Uhl GR, Sora I, Ikeda K (2004). Buprenorphine antinociception is abolished, but naloxone-sensitive reward is retained, in mu-opioid receptor knockout mice. Neuropsychopharmacology 29: 1656–1663.

Imayoshi I, Sakamoto M, Ohtsuka T, Kageyama R (2009). Continuous neurogenesis in the adult brain. Development, Growth & Differentiation 51: 379–386.

Kale SC, Lerch JP, Henkelman RM, Chen XJ (2008). Optimization of the SNR-resolution tradeoff for registration of magnetic resonance images. Hum Brain Mapp 29: 1147–1158.

Kilkenny C, Browne W, Cuthill IC, Emerson M, Altman DG (2011). Animal research: reporting in vivo experiments – the ARRIVE guidelines. J Cereb Blood Flow Metab 31: 991–993.

Kitchen I, Slowe SJ, Matthes HW, Kieffer B (1997). Quantitative autoradiographic mapping of mu-, delta- and kappa-opioid receptors in knockout mice lacking the mu-opioid receptor gene. Brain Res 778: 73–88.

LaBuda CJ, Cutler TD, Dougherty PM, Fuchs PN (2000a). Mechanical and thermal hypersensitivity develops following kainate lesion of the ventral posterior lateral thalamus in rats. Neurosci Lett 290: 79–83.

LaBuda CJ, Sora I, Uhl GR, Fuchs PN (2000b). Stress-induced analgesia in mu-opioid receptor knockout mice reveals normal function of the delta-opioid receptor system. Brain Res 869: 1–5.

Lerch JP, Yiu AP, Martinez-Canabal A, Pekar T, Bohbot VD, Frankland PW *et al*. (2011). Maze training in mice induces MRI-detectable brain shape changes specific to the type of learning. Neuroimage 54: 2086–2095.

Lewis VA, Gebhart GF (1977). Evaluation of the periaqueductal central gray (PAG) as a morphine-specific locus of action and examination of morphine-induced and stimulation-produced analgesia at coincident PAG loci. Brain Res 124: 283–303.

Linnman C, Moulton EA, Barmettler G, Becerra L, Borsook D (2012). Neuroimaging of the periaqueductal gray: state of the field. Neuroimage 60: 505–522.

Lledo PM, Saghatelyan A (2005). Integrating new neurons into the adult olfactory bulb: joining the network, life-death decisions, and the effects of sensory experience. Trends Neurosci 28: 248–254.

Lledo PM, Alonso M, Grubb MS (2006). Adult neurogenesis and functional plasticity in neuronal circuits. Nat Rev Neurosci 7: 179–193.

Ma Y, Hof PR, Grant SC, Blackband SJ, Bennett R, Slatest L *et al*. (2005). A three-dimensional digital atlas database of the adult C57BL/6J mouse brain by magnetic resonance microscopy. Neuroscience 135: 1203–1215.

Maekawa T, Tommasino C, Shapiro HM, Keifer-Goodman J, Kohlenberger RW (1986). Local cerebral blood flow and glucose utilization during isoflurane anesthesia in the rat. Anesthesiology 65: 144–151.

Manning BH (1998). A lateralized deficit in morphine antinociception after unilateral inactivation of the central amygdala. J Neurosci 18: 9453–9470.

Manning BH, Morgan MJ, Franklin KB (1994). Morphine analgesia in the formalin test: evidence for forebrain and midbrain sites of action. Neuroscience 63: 289–294.

Mansour A, Khachaturian H, Lewis ME, Akil H, Watson SJ (1987). Autoradiographic differentiation of mu, delta, and kappa opioid receptors in the rat forebrain and midbrain. J Neurosci 7: 2445–2464.

Mansour A, Fox CA, Burke S, Meng F, Thompson RC, Akil H *et al*. (1994). Mu, delta, and kappa opioid receptor mRNA expression in the rat CNS: an in situ hybridization study. J Comp Neurol 350: 412–438.

Mason P (2005). Deconstructing endogenous pain modulations. J Neurophysiol 94: 1659–1663.

May A, Hajak G, Ganssbauer S, Steffens T, Langguth B, Kleinjung T *et al*. (2007). Structural brain alterations following 5 days of intervention: dynamic aspects of neuroplasticity. Cereb Cortex 17: 205–210.

McGrath JC, Drummond GB, McLachlan EM, Kilkenny C, Wainwright CL (2010). Guidelines for reporting experiments involving animals: the ARRIVE guidelines. Br J Pharmacol 160: 1573–1576.

Nieman BJ, Lerch JP, Bock NA, Chen XJ, Sled JG, Henkelman RM (2007). Mouse behavioral mutants have neuroimaging abnormalities. Hum Brain Mapp 28: 567–575.

Pawson AJ, Sharman JL, Benson HE, Faccenda E, Alexander SP, Buneman OP *et al*. (2014). The IUPHAR/BPS Guide to PHARMACOLOGY: an expert-driven knowledge base of drug targets and their ligands. Nucleic Acids Research 42 (Database Issue): D1098–1106.

Paxinos G, Franklin KBJ (2004). The Mouse Brain in Stereotaxic Coordinates, Compact 2nd edn. Elsevier Academic Press: Boston.

Ridgway GR, Henley SM, Rohrer JD, Scahill RI, Warren JD, Fox NC (2008). Ten simple rules for reporting voxel-based morphometry studies. Neuroimage 40: 1429–1435.

Roy S, Barke RA, Loh HH (1998). MU-opioid receptor-knockout mice: role of mu-opioid receptor in morphine mediated immune functions. Brain Res Mol Brain Res 61: 190–194.

Sawiak SJ, Wood NI, Williams GB, Morton AJ, Carpenter TA (2009). Voxel-based morphometry in the R6/2 transgenic mouse reveals differences between genotypes not seen with manual 2D morphometry. Neurobiol Dis 33: 20–27.

Schwartz MW, Woods SC, Porte D Jr, Seeley RJ, Baskin DG (2000). Central nervous system control of food intake. Nature 404: 661–671.

Sora I, Funada M, Uhl GR (1997a). The mu-opioid receptor is necessary for [D-Pen2,D-Pen5]enkephalin-induced analgesia. Eur J Pharmacol 324: R1–R2.

Sora I, Takahashi N, Funada M, Ujike H, Revay RS, Donovan DM *et al*. (1997b). Opiate receptor knockout mice define mu receptor roles in endogenous nociceptive responses and morphine-induced analgesia. Proc Natl Acad Sci U S A 94: 1544–1549.

Sora I, Elmer G, Funada M, Pieper J, Li XF, Hall FS *et al*. (2001). Mu opiate receptor gene dose effects on different morphine actions: evidence for differential in vivo mu receptor reserve. Neuropsychopharmacology 25: 41–54.

Sora I, Ikeda K, Mishina Y (2003). Receptor knock-out and gene targeting. Generation of knock-out mice. Methods Mol Med 84: 205–216.

Sumiyoshi A, Riera JJ, Ogawa T, Kawashima R (2011). A mini-cap for simultaneous EEG and fMRI recording in rodents. Neuroimage 54: 1951–1965.

Sun YG, Lundeberg T, Yu LC (2003). Involvement of endogenous beta-endorphin in antinociception in the arcuate nucleus of hypothalamus in rats with inflammation. Pain 104: 55–63.

van de Ven RC, Hogers B, van den Maagdenberg AM, de Groot HJ, Ferrari MD, Frants RR *et al*. (2007). T(1) relaxation in in vivo mouse brain at ultra-high field. Magn Reson Med 58: 390–395.

Wang SX, Chen JX, Yue GX, Bai MH, Kou MJ, Jin ZY (2012). Xiaoyaosan decoction regulates changes in neuropeptide y and leptin receptor in the rat arcuate nucleus after chronic immobilization stress. Evid Based Complement Alternat Med 13: 1–16.

Yang D, Li Q, Fang L, Cheng K, Zhang R, Zheng P *et al*. (2011). Reduced neurogenesis and pre-synaptic dysfunction in the olfactory bulb of a rat model of depression. Neuroscience 192: 609–618.

Yang ZJ, Tang JS, Jia H (2002). Morphine microinjections into the rat nucleus submedius depress nociceptive behavior in the formalin test. Neurosci Lett 328: 141–144.

Yuste R, Bonhoeffer T (2001). Morphological changes in dendritic spines associated with long-term synaptic plasticity. Annu Rev Neurosci 24: 1071–1089.

Zagon IS, McLaughlin PJ (1983). Increased brain size and cellular content in infant rats treated with an opiate antagonist. Science 221: 1179–1180.

Zagon IS, Gibo DM, McLaughlin PJ (1992). Ontogeny of zeta (zeta), the opioid growth factor receptor, in the rat brain. Brain Res 596: 149–156.

Zagon IS, Verderame MF, McLaughlin PJ (2002). The biology of the opioid growth factor receptor (OGFr). Brain Res Brain Res Rev 38: 351–376.